Available online at www.sciencedirect.com
SCIENCE DIRECT
Catalysis Today 109 (2005) 61–68
CATALYSIS TODAY
www.elsevier.com/locate/cattod

Maya crude hydrodemetallization and hydrodesulfurization catalysts: An effect of TiO_2 incorporation in Al_2O_3

Mohan S. Rana *, J. Ancheyta, S.K. Maity, P. Rayo

Instituto Méxicano del Petróleo, Eje Central Lázaro Cárdenas 152, México D.F. 07730, México

Available online 10 October 2005

Abstract

Hydrotreating of Maya heavy crude oil over high specific surface area CoMo/TiO_2–Al_2O_3 oxide supported catalysts was studied in an integral reactor close to industrial practice. Activity studies were carried out with Maya crude hydrodesulfurization (HDS), hydrodemetallization (HDM), hydrodenitrogenation (HDN), and hydrodeasphaltenization (HDAs) reactions. The effect of support composition, the method of TiO_2 incorporation, and the catalyst deactivation are examined. Supported catalysts are characterized by BET specific surface area (SSA), pore volume (PV), pore size distribution (PSD), and atomic absorption. It has been found that sulfided catalysts showed a wide range of activity variation with TiO_2 incorporation into the alumina, which confirmed that molybdenum sulfided active phases strongly depend on the nature of support. The pore diameter and nature of the active site for HDS, HDM, HDN, and HDAs account for the influence of the large reactant molecules restricted diffusion into the pore, and/or the decrease in the number of active sites due to the MoS_2 phases buried with time-on-stream. The textural properties and hysteresis loop area of supported and spent catalysts indicated that catalysts were deactivated at the pore mouth due to the metal and carbon depositions. The atomic absorption results agreed well regarding the textural properties of spent catalysts. Thus, incorporation of TiO_2 with γ-Al_2O_3 alters the nature of active metal interaction with support, which may facilitate the dispersion of active phases on the support surface. Therefore, the TiO_2 counterpart plays a promoting role to HDS activity due to the favorable morphology of MoS_2 phases and metal support interaction.

Keywords: HDM; HDS; HDN; HDAs; Maya crude; TiO_2–Al_2O_3; CoMo catalyst; Deactivation; Heavy oil HDT; Support effect

1. Introduction

Hydrotreating is one of the most important processes in the petroleum refinery, because it is a process which mainly removes sulfur, nitrogen, and unwanted metals from hydrocarbons [1]. These molecules are the main source of environmental pollution, and also poison the catalysts used in various refineries operations [2]. For instance, metals need to be removed from hydrocarbons because they poison the catalyst and may cause corrosion even in minor quantities. During the hydrodemetallization, nickel and vanadium form sulfides, which results in pore mouth plugging and decreases catalytic activity by restricting the access of reactants to the catalytic sites. Thus, in the case of heavy oil processing, pore diameter is of equal importance as the active sites. A large variety of sulfur, nitrogen, and organometallic species, together with large molecules of asphaltenes, are present in heavy oil, which constitute the heaviest molecule in crude and are also responsible for catalyst deactivation during the hydrotreating processes [3]. Therefore, it is essential to conserve the catalysts using the meso or macro-porous and put them to maximum possible use with highly dispersed active sites.

Support effect in hydrotreating [4–6] catalysis, especially TiO_2 incorporation in alumina, is well reported for model molecules [7–13], but there is limited use of these catalysts in commercial studies [14,15]. However, due to the strength, low surface area, low pore volume, and high cost, pure TiO_2 is not a favorable support [16,17]. To overcome these problems, TiO_2 incorporation into the different oxides such as ZrO_2 [18], SiO_2 [19], and Al_2O_3 [7–13], was studied to modify the physicochemical support properties. Apart from the wide range of studies using different model molecules and characterization on the TiO_2–Al_2O_3 supported catalyst, the application of this material in heavy oil hydrotreating is not common, with the exception of a few publications from our group [14,15], where

* Corresponding author. Tel.: +52 55 9175 8418; fax: +52 55 9175 8429.
E-mail address: msingh@imp.mx (M.S. Rana).

0920-5861/$ – see front matter © 2005 Elsevier B.V. All rights reserved.
doi:10.1016/j.cattod.2005.08.016

we have reported that TiO_2–Al_2O_3 supported catalysts showed higher activity than reference catalysts. However, the stability of these catalysts was not as expected. That could be due to the support preparation, since the use of aluminum sulfate [15] as alumina source may generate strong acidity on a sulfided catalyst, if there were some SO_4^- ions remaining in catalyst; or, another reason is the feed composition employed in those studies [14,15], which could deactivate the catalyst at a very fast rate due to the precipitation of asphaltene in naphtha. Regarding to this aspect, Rayo et al. [14] presented a nice report about the effect of feed dilution on NiMo/Al_2O_3–TiO_2 supported catalysts.

In the present work, the effect of TiO_2 incorporation into the Al_2O_3 using different methods such as urea hydrolysis, ammonia hydrolysis, incipient wetness impregnation, and delayed precipitation of titania is reported. Among these techniques, urea hydrolysis offers advantages for hydrogenolysis (HDS, HDN, and HDM) activities while the delayed precipitation method showed lower activity due to the lower average pore diameter of the catalyst. However, the effect of individual activity on different catalysts is not very clear due to the similar composition of TiO_2 and Al_2O_3 [i.e. $TiO_2/TiO_2 + Al_2O_3 \approx 0.1$]. Different methods of support preparation showed variation in PSD, which may also cause some differences between the activities. The effect of PSD is confirmed by the comparison of fresh and spent catalyst textural properties as well as deposited metals. An increase in the hysteresis loop area is calculated and the results are discussed as an effect of metal poisoning and coke deposition near the pore mouth of catalyst after 120 h TOS.

2. Experimental

Al_2O_3–TiO_2 supports were prepared by using different methods employing aluminum nitrate solution (~1.5 M) and titanium tetra chloride or titanium *iso*-propoxide as source of Al_2O_3 and TiO_2, respectively. The composition of TiO_2 in the support was kept low (i.e. 10 wt.%) due to commercial importance of the catalyst. The Al_2O_3–TiO_2 sample is represented as AT, where different preparation methods will be indicated by 1, 2, 3, 4, 5, and 6.

1. AT-1 and AT-2, urea and ammonia hydrolysis co-precipitation methods respectively, which are reported in detail elsewhere [20]. Prior to the precipitation, the aqueous solution of $TiCl_4$ and aluminum nitrate was mixed together.
2. AT-3 is also similar to the ammonia precipitation except for the fact that the precursor of Ti is titanium *iso*-propoxide instead of $TiCl_4$.
3. AT-4 is titanium *iso*-propoxide, impregnated using incipient wetness impregnation over the γ-Al_2O_3 (550 °C).
4. AT-5 is titanium *iso*-propoxide, impregnated using incipient wetness impregnation over the boehmite phase of alumina (AlOOH).
5. AT-6, the urea hydrolysis delayed precipitation of TiO_2, aluminum nitrate was first precipitated, and after 30 min titanium *iso*-propoxide, considering the titania precipitates on the surface of the alumina particle.

The above calcined (550 °C) supports prepared with different methods were analyzed by atomic absorption and their compositions are reported in Table 1.

The molybdenum-supported catalysts were prepared using the incipient wetness impregnation method. An appropriate amount of ammonium heptamolybdate (AHM) (Fluka AR grade) was used and dissolved in ammoniac solution. The Co-promoted catalyst was also prepared by the sequential impregnation procedure on the Mo-loaded catalyst (dried at 120 °C and calcined at 400 °C). The cobalt nitrate salt was impregnated in aqueous medium. The final catalyst was dried in presence of air at 120 °C overnight and calcined at 450 °C for 4 h. The compositions of the supported catalysts are also reported in Table 1.

The BET SSA, PV and PSD analyses were carried out in Quantachrome Nova 2000 equipment. Nitrogen gas was employed for SSA measurements at liquid nitrogen temperature (−196 °C). Prior to the adsorption, the samples were degassed 3 h at 300 °C. X-ray power diffraction (XRD) patterns were collected on a Siemens D500 diffractometer using Cu Kα radiation.

The feedstock contains 50/50 (w/w) of Maya crude and diesel. Diesel was used as a diluent to avoid gum formation during processing. The feed composition is presented in Table 2. Metals (Ni, V) were analyzed in the feed and products using flame atomic absorption spectrometry (ASTM D 5863-00a method). The total S content was analyzed with the HORIBA model SLFA-2100/2800 using scattered spectroscopy by sulfur, generating energy dispersive X-ray fluorescence. The X-ray beam was separated selectively with the help

Table 1
Composition and textural properties of supported catalysts

Catalysts	Support $Al_2O_3/(Al_2O_3 + TiO_2)$	Catalyst composition (wt.%)		Textural properties		
		Co	Mo	SSA (m^2/g)	PV (ml/g)	APD (nm)
AT-1	0.908	2.13	5.53	230	0.4372	7.4
AT-2	0.901	2.16	5.52	255	0.4100	6.8
AT-3	0.902	2.25	5.53	260	0.3319	5.5
AT-4	0.906	2.20	5.50	206	0.3200	5.8
AT-5	0.905	2.21	5.65	232	0.3426	5.7
AT-6	0.911	2.02	5.57	231	0.3085	4.1

Table 2
Physico-chemical characterization of feed

Properties	(Maya crude + diesel) (50/50, w/w)
Elemental analysis (wt.%)	
C	84.2
H	8.8
N	0.184
S	2.21
Metal (wppm)	
Ni	26.21
V	124.78
(Ni + V)	150.99
Ca	5.0
Mg	1.01
Na	21.2
K	10.2
Fe	1.02
Asphaltene (wt.%) (n-C_7 insol.)	8.43
Physical properties	
Density, 20/4 °C	0.88
Pour point (°C)	−15
Ramscarbon (wt.%)	5.45
API gravity	30.09
Viscosity (g/cm s) at 100 °C	9.45

of a filter and detected as sulfur concentration. Nitrogen was measured by oxidative combustion and chemiluminescence (ASTM D 4629-02 method) at high temperature combustion in an oxygen rich atmosphere. Asphaltene is defined as the insoluble fraction in *n*-heptane. The solid carbonaceous material on spent catalysts (toluene washed) was analyzed with a Leco SC-444 instrument using the ASTM C 1408-98 method with direct combustion-infrared detection.

The catalyst pretreatment and the hydrotreating reactions were carried out in a high pressure fixed-bed up flow micro reactor. A 10 ml (≈8 g) oxidic catalyst was sulfided in situ with a mixture of dimethyldisulfide (DMDS), straight run gas oil (SRGO), and H_2. The details of sulfidation were given elsewhere [20,21]. After sulfidation, the flow was switched to the test feed (Table 2) and the following operating conditions were adjusted: catalyst bed temperature of 380 °C, LHSV of 1 h^{-1}, H_2/HC 356 m^3/m^3, and pressure of 5.4 MPa.

3. Results and discussion

3.1. Textural properties of catalysts and their composition

More than any other characteristic, the textural properties of a catalyst, such as pore volume, pore size distribution, and pore nature, are some of the most important properties of a heavy oil hydrotreating catalyst. The textural properties of catalysts were characterized using nitrogen adsorption–desorption isotherms as shown in Fig. 1, and the results are reported in Table 1. All catalysts are high specific surface (SSA) in nature and contain a total pore volume in the range of 0.3–0.4 ml/g. The specific area of TiO_2–Al_2O_3 supports is comparable to γ-Al_2O_3 i.e., 200–250 m^2/g. The hysteresis loop indicated that catalysts are mesoporous in nature, which is the characteristic feature of a Type IV

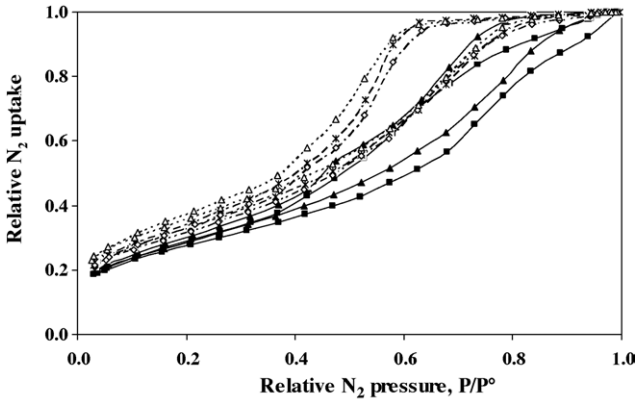

Fig. 1. Nitrogen adsorption–desorption isotherms of supported catalysts: (■) AT-2; (▲) AT-3; (□) AT-4; (◇) AT-5; (△) AT-6.

isotherm. However, the exact shape of the loop varies from one catalyst to another, which indicated that the geometry of pores is not the same for all catalysts. The catalysts supported on AT-1, AT-2, and AT-3 represent slightly different hysteresis, as catalyst pore size distribution is more towards the macro type of pores. Similar results can be obtained using BJH pore size distributions derived from the adsorption data which are presented in Fig. 2, these complementary results indicated that the 15, 3, and 12% of pores lies in the range of 20–100 nm for AT-1, AT-2, and AT-3 as shown more clearly in Fig. 2 inset. Therefore, as an effect of the different preparation method or titania precursor the delayed precipitation and incipient wetness impregnation of titania represent a smaller pore diameter. However, titania precursors, such as titanium tetra chloride and titanium (IV) *iso*-propoxide (AT-2 and AT-3, respectively), as well as co-precipitations of titania with alumina using urea and ammonia as a precipitating agent (AT-1 and AT-2, respectively), showed a small difference in textural properties.

X-ray diffractograms (not shown) for different supports containing TiO_2 and CoMo supported catalysts were recorded, but they showed only reflections corresponding to γ-Al_2O_3 that could be due to the TiO_2 or CoMo phases well dispersed over

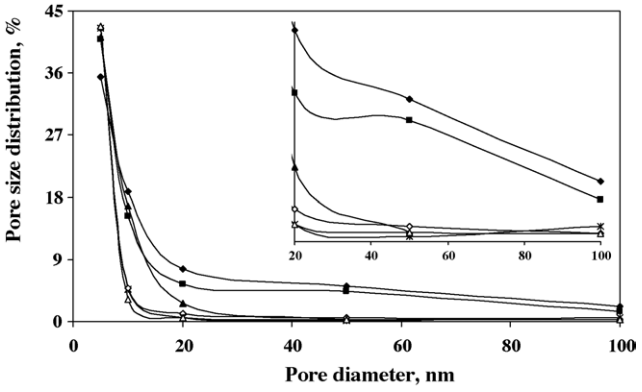

Fig. 2. Pore size distribution of supported catalysts: (◆) AT-1; (■) AT-2; (▲) AT-3; (□) AT-4; (◇) AT-5; (△) AT-6.

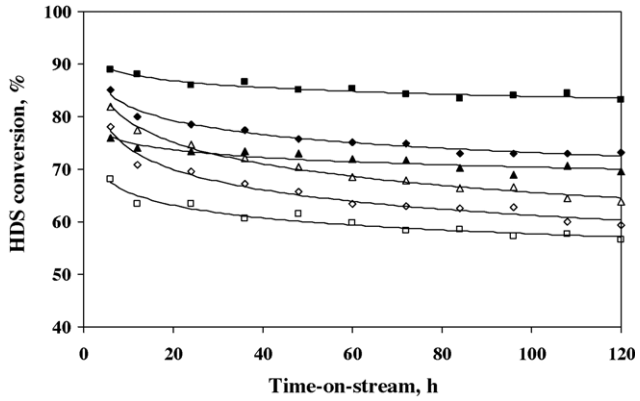

Fig. 3. HDS conversion with time-on-stream: (◆) AT-1; (■) AT-2; (▲) AT-3; (□) AT-4; (◇) AT-5; (△) AT-6.

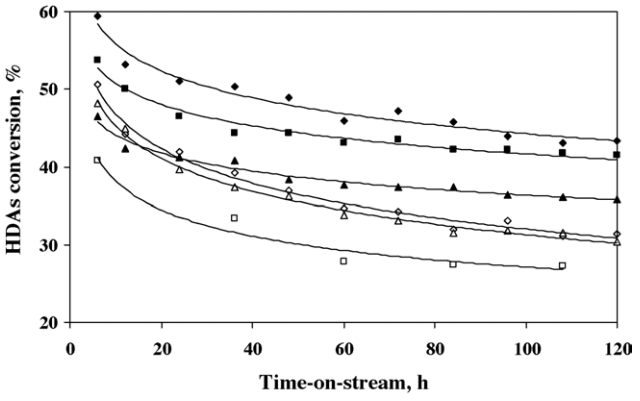

Fig. 5. HDAs conversion with time-on-stream: (◆) AT-1; (■) AT-2; (▲) AT-3; (◇) AT-5; (△) AT-6.

the γ-Al_2O_3, and no cluster formation has been detected, or their crystal size was lower than 4 nm.

3.2. Activities

The results from the different activities, such as HDS, HDN, HDAs, and HDM, for different catalysts against TOS are reported in Figs. 3–6. To extract the effect of the TiO_2 incorporation method and its precursor, the catalytic performance of MoS_2-based catalysts depends on their morphology and the orientation of active sites on the support surface [22]. Considering the effect of different methods, prepared Al_2O_3–TiO_2 support has structural variation in the orientation of TiO_2 and so do the active metal phases. However, due to the complex nature of feedstock composition and its product analysis, it is very difficult to assess the small effect of support on catalytic activities. Nevertheless, the effect is demonstrated for each catalytic function. The catalytic activities were carried out with the feedstock containing 50 wt.% Maya crude and 50 wt.% diesel (solvent); therefore, the pore size distribution may not affect at the initial conversion due to the dilution, while with time-on-stream due to pore mouth plugging the diffusion becomes more prominent, especially for HDM and HDAs.

The hydrodesulfurization result in Fig. 3 indicates that the incorporation of TiO_2 produces important changes in the support surface, and as result, HDS catalytic site enhancements. The ammonia prepared (AT-2) CoMo supported catalyst showed better and more stable conversion as a function of time-on-stream. However, the similarly prepared support (AT-3) using titanium (IV) *iso*-propoxide (Ti-iProO) as a titanium source showed much less HDS activity with similar stability to TOS. These results indicate that the $TiCl_4$ precipitation is more homogeneous than the Ti-iProO, due to the better ionization capacity of $TiCl_4$ salts in comparison with the Ti-iProO. Apart from that, during the final calcination of support, the nature of the OH groups, which are responsible for the different interaction with the Mo atoms, varied [5,8] during the impregnation. Other supported catalysts are comparatively less active for HDS, and activity decreases in AT-6, AT-5, and AT-4. The stabilities of these catalysts are almost the same, except for AT-6. Surprisingly, the delayed precipitation (AT-6) showed good initial activity, but it decreases faster than the others. This might be due to the excess TiO_2 precipitation on the surface of the alumina and the rapid loss of active sites.

The hydrodenitrogenation (HDN) results against time-on-stream are shown in Fig. 4, which follow a similar tendency to

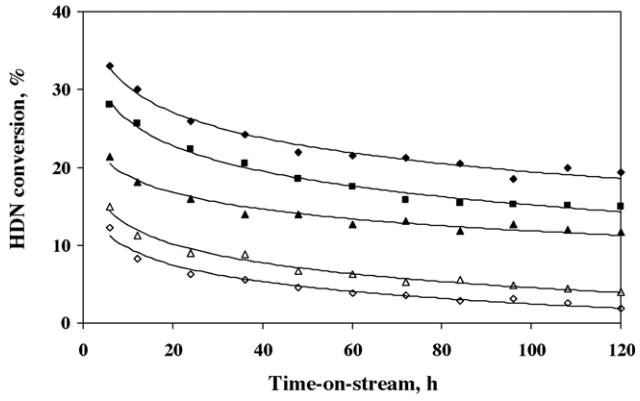

Fig. 4. HDN conversions with time-on-stream: (◆) AT-1; (■) AT-2; (▲) AT-3; (◇) AT-5; (△) AT-6.

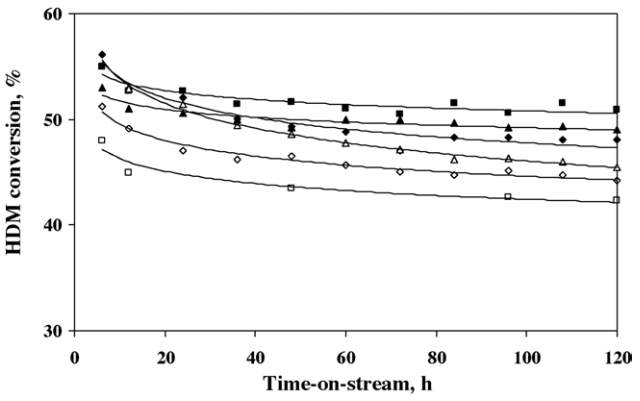

Fig. 6. HDM conversions with time-on-stream: (◆) AT-1; (■) AT-2; (▲) AT-3; (□) AT-4; (◇) AT-5; (△) AT-6.

those discussed for HDS, except for AT-1 which exhibited slightly better HDN activity than the other catalysts. However, the conversion of HDN is much less than that of HDS; thus, the sum of catalytic sites is not the same as for HDS. Another possible reason for this is that textural properties might have a role in restricting the complex organo-metallic molecules, which are mainly constituents of a porphyrinic structure. With TOS, a similar trend of deactivation indicated that the number of catalytic sites is deactivated or varied similarly. The surprising behavior for HDN activity in the case of AT-1 must be due to other parameters, such as support acidity, which may enhance the HDN conversion [23]. Recently, Inoue et al. [24] reported that, by comparison, the $CoMo/TiO_2$-based catalyst is a much better choice for straight-run gas oil HDN than HDS using commercial $CoMo/Al_2O_3$ and $NiMo/Al_2O_3$ catalysts. The acidity of this support/catalyst is expected to be slightly more due to the urea hydrolysis slow precipitation of TiO_2 and Al_2O_3 [20], which is expected to have higher number of Ti–O–Al bonds.

As shown in Fig. 5, the hydrodeasphaltenization (HDAs) conversion followed the similar trends exactly as we observed for HDN activity with time-on-stream. The decrease in activity with time also followed the same tendency. In the case of HDAs, deactivation is slightly complicated due to the cracking of asphaltene, which deactivates the acidic sites faster than the metallic sites ($Co–MoS_2$). However, the conversion of asphaltene molecules proceeds via hydrogenation, followed by cracking. We suppose that the plausible factor affecting the reactivities of the AT-1 is the catalyst acidity and the nitrogen ring (porphyrin) selective adsorption on the surface of the catalyst [25]. This is in line with the common knowledge that deactivation of a heavy oil hydrotreating catalyst can occur in several ways: either by the carbon deposition on the catalytic site/acidic site, by the deposition of metal (V + Ni) over the existing active site (CoMoS), or by the pore plugging due to the metal and carbon depositions [2,20,26,27].

The hydrodemetallization (HDM) conversions for different catalysts are reported in Fig. 6 as a function of time-on-stream. The tendency for HDM activity is similar to that presented for HDS conversion. This could be due to the hydrogenolysis route followed by both reactions, since the contrary behavior of HDN and HDAs may be due to the π-electrons affinity for the porphyrin ring to the Brønsted or Lewis acid sites. Except for AT-6, which deactivated faster than the other catalysts, the stability with time varies marginally with a different method of Ti incorporation in the support. The stability of AT-6 also corresponds to the pore size distribution, which possess 4.1 nm average pore diameter. Similar deactivation is observed for this catalyst in the case of HDAs. In other words, the asphaltene and metal reactant molecules are restricted due to the diffusion into the pores. On the other hand, the smaller pore diameter catalyst deactivated faster due to the plugging of the pore mouth. Recently, we published [20] similar results for the γ-Al_2O_3 supported catalyst which indicated that the smaller the pore diameter, the faster the deactivation with time-on-stream. Apart from this catalyst, the TiO_2 incipient wetness impregnation method prepared catalysts (AT-4 and AT-5) are less active (HDS, HDM and HDAs) than AT-1, AT-2, and AT-3 catalysts. This can be explained on the basis of pore size distribution which is given in Table 1. The effect of impregnation between two catalysts (AT-4 and AT-5) also clearly indicated that Ti incorporation un-calcined alumina (boehmite phase) showed better activity than the γ-Al_2O_3 modified supported catalyst, which is most likely due to the interaction of the boehmite (AlOOH) –OH group with titania.

The constant HDS and HDM conversions in comparison with HDN and HDAs for AT-2 and AT-3 catalysts may indicate the optimum pore diameter for this kind of feedstock, thus showing the stable activity with TOS. On the other hand, HDN activity decreases with TOS in all catalysts, which could be due to the adsorption properties of organic nitrogen compounds (porphyrins) on the surface of catalyst. One more possible explanation is the acidity of the mixed oxide supported catalyst [25], which is prone to nitrogen adsorption, and the fact that these acid sites are decreasing with TOS faster than metallic sites (hydrogenolysis); therefore, a continuous decrease can be observed for HDN conversion with TOS. These results are further supported by the conversion of the HDAs, which may also crack on the same acid sites. Thus, heavy oil hydroprocessing catalyst acidity plays an important role in deactivating the catalyst.

3.3. Spent catalysts textural properties

The decreases of HDS, HDAs, and HDM activities with time-on-stream are not only due to the deactivation of active sites, but also to metal deposition on the catalyst surface. In general, the hydrotreating catalyst life is more than 2 years if the feedstock is light oil; but when using heavy oil, catalyst stability, which mostly depends on the pore size distribution of the catalyst, is very low. The effect of pore size distribution has been studied by several authors [28–30]. It is reported that the HDM catalyst should be macro-porous in nature; on the other hand, after a certain limit the HDS activity decreases when the pore diameter increases [20,31]. Therefore, a balance catalyst that uses surface area and pore diameter as important parameters should be considered. The challenging task in heavy oil processing is the catalyst specifications, which will vary with refinery location or feedstock [32]. Nevertheless, we tried to determine the deactivation of our catalysts semi-quantitatively using very simple experiments of N_2 adsorption–desorption isotherm area as shown in Fig. 7. However, this kind of deactivation is only valid for deposition of metal and carbon at the pore mouth, which is reported in most of the literature [33–36]. The large increase in hysteresis area is an indication for deactivation via the pore mouth and the results are shown in Table 3. An increase in isotherm area is due to the change of cylindrical pores into the ''ink-bottle'' type of pores [26,37]. The increase in area is well correlated with the percentage decrease (50–80%) in the specific surface area and total pore volume of spent catalysts after 120 h time-on-stream. The average pore diameter of the spent catalyst showed irregular behavior due to the way it is calculated with the equation

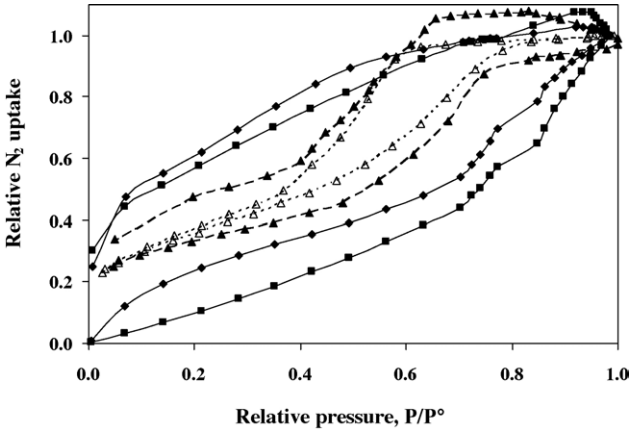

Fig. 7. Fresh and spent catalysts adsorption desorption isotherms: (△) CoMo/AT-1-Fresh catalyst; (□) AT-1-WW (spent catalyst without wash); (◇) AT-1 (spent catalyst washed with toluene).

[$r_p = 2V_{liq.}/S$, where r_p = average pore diameter, $V_{liq.}$ = volume of liquid nitrogen ($V_{liq.} = P_a V_{ads} V_m/RT$, ambient conditions) and S is BET surface area] which is only valid for cylindrical pores [38]. Therefore, the only possible option to measure the spent catalyst textural properties is to use the isotherm area and percentage decrease in SSA and PV. The data indicated extensive changes in textural properties of catalysts. These changes are also supported by the atomic absorption data of spent catalysts as reported in Table 4. The deposition of carbon and V is more obvious, while Ni is deposited in almost the same quantity for all catalysts. These results correspond to the catalyst after 120 h TOS, refluxed (washed) with toluene, and dried at 200 °C. To see the effect of washing, analysis of one catalyst without washing (AT-1-WW) is also reported. This indicated that the carbon and S/Mo ratio decrease due to the very small quantity of soft coke that may dissolve in toluene and the exchange of S atoms with the oxygen. These results indicated that the bigger the pore diameter, the higher the metal retention capacity. Metal retention capacity can also be confirmed by the S/Mo ratio that decreases with pore diameter, while using the theoretical value for a sulfided catalyst, this ratio should be around 2 [39].

The above results confirmed that catalyst deactivation and pore plugging are carried out by carbon and metal deposition.

Table 3
N_2 adsorption–desorption hysteresis loop area analysis

Catalyst	Absolute hysteresis loop area		
	Fresh catalyst	Spent catalyst	Increase (%)
AT-1-WW	–	0.3173	19.8
AT-1	0.1191	0.2765	15.7
AT-1-R	–	0.1809	6.2
AT-2	0.1067	0.2227	11.6
AT-3	0.1144	0.2358	12.1
AT-4	0.1202	0.2502	12.9
AT-5	0.1248	0.2558	13.1
AT-6	0.1254	0.2509	12.5

AT-1-WW: catalyst without washing; AT-1-R: catalyst regenerated.

Table 4
Atomic absorption analysis of spent catalysts

Catalyst	wt.%						S/Mo (mol/mol)
	Mo	Co	Ni	V	C	S	
AT-1-WW	2.85	1.556	0.106	0.563	11.44	3.72	3.91
AT-1	2.98	1.0707	0.116	0.521	10.08	3.1	3.12
AT-1-R	5.40	1.8511	0.152	0.556	0.01	–	–
AT-2	3.48	1.476	0.110	0.501	9.54	3.51	3.03
AT-3	4.62	1.300	0.112	0.513	9.99	3.90	2.53
AT-4	3.50	1.350	0.110	0.440	9.88	3.50	3.00
AT-5	4.68	1.262	0.142	0.368	9.10	3.40	2.18
AT-6	4.63	1.305	0.195	0.420	9.30	3.66	2.37

AT-1-WW: catalyst without washing; AT-1-R: catalyst regenerated.

To obtain better insights between carbon and metal depositions we tried to distinguish the deactivation by carbon or metals by removing the deposited carbon. Thus, one catalyst was regenerated and its textural properties are compared with the fresh and spent catalysts in Table 3 and Fig. 1. It is expected that carbon deposition may take place throughout the catalyst surface, or most likely on acid sites (support and sulfided catalysts), while metal deposition preferred being near the pore mouth and over the coordinated unsaturated site. Textural properties of a regenerated catalyst (CoMo/AT-1-R) indicated that almost 70–75% of the pores can be reproduced during the regeneration but 25–30% of the pores, which can be called metal deactivated pores, remain unaffected. No more carbon is detected after regeneration (at 550 °C for 8 h in the presence of oxygen); therefore, now only deposited metals have an effect on textural properties, as shown in Table 3. However, the position of metals may not be the same as in the un-regenerated catalyst (spent catalyst). The recovery of surface area and pore volume is around 70 and 50% respectively, which is low. Therefore, the textural properties of the regenerated catalyst cannot be 100% recovered unless deposited metals (Ni + V) could be separated, which appears to be an almost impossible task during the in situ regeneration. The atomic absorption analyses of deposited metals (V and Ni) for regenerated catalysts are shown in Table 4. In the case of the regenerated catalyst, an increase in the Co, Mo, etc. metals is observed due to the decrease of carbon percentage in the catalyst (i.e., the real composition of the spent catalyst in an oxide state).

We have tried to calculate the BJH adsorption and desorption surface areas to find another explanation for the formation of ''ink-bottle'' types of pores due to the deposition at the pore mouth. In Table 5, the ratio for desorption area and BET–SSA and/or desorption area (D)/adsorption area (A) for fresh catalysts remains constant at around 1.1 considering that all pores are cylindrical in nature. On the other hand, spent catalysts desorption area/BET–SSA ratio increases as the pore plugging increases. We conclude this effect as:

(i) D/A close to unity, the pores are cylindrical in nature,
(ii) D/BET–SSA greater than one, more deactivated pore at the pore mouth,

Table 5
N_2 adsorption–desorption measurements of pore mouth plugging

Catalysts	Fresh catalyst			Spent catalyst				
	D/*A*	*D*/BET	*A*/BET	SSA	PV	*D*/*A*	*D*/BET	*A*/BET
TA-1-WW	–	–	–	82	0.099	2.60	4.11	1.58
AT-1	1.2	1.4	1.19	115	0.119	2.41	2.96	1.23
AT-1-R	–	–	–	158	0.229	1.30	1.4	1.07
AT-2	1.2	1.5	1.22	88	0.271	1.37	1.78	1.31
AT-3	1.2	1.4	1.19	82	0.301	1.33	1.69	1.27
AT-4	1.2	1.3	1.13	102	0.090	1.35	1.70	1.20
AT-5	1.2	1.4	1.14	107	0.171	1.23	1.52	1.24
AT-6	1.2	1.4	1.18	106	0.172	1.35	1.39	1.03

Specific surface area (SSA) (m^2/g); PV (ml/g). APD = average pore diameter, nm. *A* = pore area calculated from BJH adsorption; *D* = pore area calculated from desorption. BET = total BET surface area. Spent catalyst (120 h TOS). AT-1-WW: catalyst without washing. AT-1-R: catalyst regenerated.

(iii) *A*/BET–SSA ratio should not be affected by the pore plugging and catalyst deactivation.

Therefore, the BJH desorption area is affected by the geometry of pores, while the adsorption area looks unaffected by the pore geometry and the catalyst deactivation. The regenerated catalyst also followed the same principle of deactivation and indicated that around 60% of pore plugging can be recovered at our regeneration conditions.

These results are also supported by the activities results, which vary with the modifications of the surface where the existence of deposited metal sulfide is suggested. The variation of conversion changes with the progress of time and deposited metals, the latter is being mainly affected by the porosity of the catalyst. As shown in Fig. 8, a comparison between the hydrogenolysis (C–S, C–M, where M is V and Ni metals) selectivity indicated that these catalysts are selectively good for

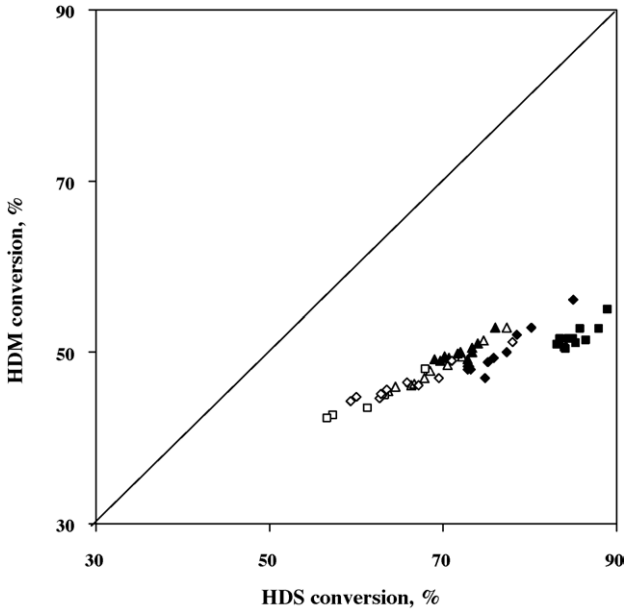

Fig. 8. HDM and HDS selectivities: (◆) AT-1; (■) AT-2; (▲) AT-3; (□) AT-4; (◇) AT-5; (△) AT-6.

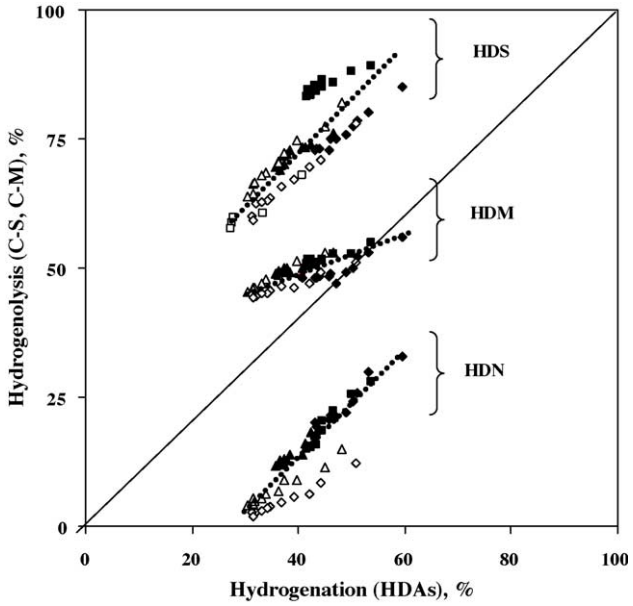

Fig. 9. Relationship between the hydrogenolysis (C–S, C–N, C–M) and hydrogenation (HDAs) functionalities: (◆) AT-1; (■) AT-2; (▲) AT-3; (□) AT-4; (◇) AT-5; (△) AT-6.

HDS. The selectivity for hydrogenolysis/hydrogenation is plotted in Fig. 9. The HDM selectivity remains more or less constant with HDAs conversion, while HDS and HDN vary proportionally with HDAs conversion. The different magnitude of activity variation also represents the diffusion limitations for HDM molecules. Since sulfur molecules initially do not depend on the pore diameter, the conversion is high, but the number of catalytic sites decreases due to the deposited metal and carbon, and the activity decline is much faster than HDM. Thus, the HDM activity is less sensitive to the active site, but more controlled by the pore diameter.

The comparison between the TiO_2 containing catalyst as well as pure alumina supported catalyst conversions after 120 h TOS are shown in Fig. 10. In all cases, the initial conversion

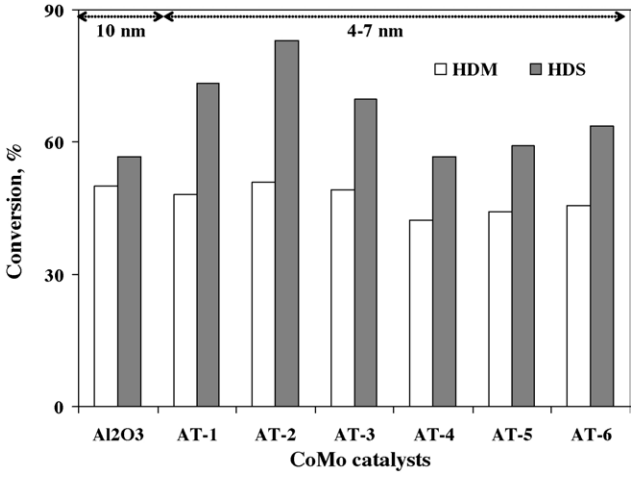

Fig. 10. Comparison between HDS and HDM conversion over CoMo supported catalysts as a function of TiO_2 incorporation in support.

was higher for TiO_2–Al_2O_3 supported catalysts than the alumina supported catalyst, and the results of initial conversion are not justifiable data for heavy oil processing. The TiO_2 containing catalyst enhances HDS activity due to the structural promotional effect of TiO_2 in the support. On the other hand, after 120 h TOS, HDM conversion either remains the same as in alumina or slightly decreases by the incorporation of TiO_2, which seems to be an effect of average pore diameter (APD) or stability of the catalysts. The mixed oxide supported catalysts have an APD between the 4 and 7 nm, while the alumina supported catalyst has a 10 nm pore diameter, which might have a corresponding effect on the stability of the catalyst.

4. Conclusions

The effect of TiO_2 incorporation in alumina via different methods was studied in this work, and better textural properties of Al_2O_3–TiO_2 mixed oxide support were obtained with urea hydrolysis prepared support. The incipient wetness impregnation method decreases the number of pores as well as the average pore diameter of the support. CoMo supported catalysts showed a wide range of activity variation as a function of TiO_2 incorporation into the alumina, which relishes the fact that molybdenum sulfided active phases strongly depend on the nature of the support. Therefore, a TiO_2 counterpart plays a structural role to the catalyst, provides high intrinsic activity, and generates favorable morphology of MoS_2 phases and metal support interaction. The textural properties of the supported and spent catalysts hysteresis loop area indicated that catalysts were deactivated at the pore mouth due to the metal and carbon depositions. The atomic absorption results are complementary to the textural properties of the spent catalysts. The selectivity results indicated that these catalysts are good for HDS reaction but not for HDM, which requires a higher average pore diameter and macro pore size distribution.

Acknowledgements

We thank I.M.P. for financial support. We also express our appreciation to Mr. José G. Espinosa and Mrs. Bertha Núñez for helping with the preparation of feedstock and adsorption–desorption experiments.

References

[1] H. Topsøe, B.S. Clausen, F.E. Massoth, in: J.R. Anderson, M. Boudart (Eds.), Hydrotreating Catalysis—Science and Technology, vol. 11, Springer-Verlag, New York, 1996.
[2] E. Furimsky, F.E. Massoth, Catal. Today 52 (1999) 381.
[3] J.W. Gosselink, CatTech 2 (1998) 127.
[4] M. Breysse, J.L. Portefaix, M. Vrinat, Catal. Today 10 (1991) 489.
[5] F. Luck, Bull. Soc. Chim. Belg. 100 (1991) 781.
[6] M.S. Rana, B.N. Srinivas, S.K. Maity, G. Murali Dhar, T.S.R. Prasada Rao, Stud. Surf. Sci. Catal. 127 (1999) 397.
[7] Y. Saih, K. Segawa, Catal. Today 86 (2003) 61.
[8] E. Olguin, M. Vrinat, L. Cedeno, J. Ramirez, A. Lopez-Agudo, Appl. Catal. A 165 (1997) 7.
[9] C. Pophal, F. Kameda, K. Hosino, S. Yoshinaka, K. Segawa, Catal. Today 39 (1997) 21.
[10] E. Rodenas, T. Yamaguchi, H. Hattori, K. Tanabe, J. Catal. 69 (1981) 434.
[11] W. Zhaobin, X. Quin, G. Xiexian, E.L. Sham, P. Grange, B. Delmon, Appl. Catal. A 75 (1991) 171.
[12] C. Lahousse, F. Mauge, J.C. Lavalley, J. Bachelier, J. Chem. Soc. Far. Trans. 91 (17) (1995) 907.
[13] M. Breysse, P. Aanasiev, C. Geantet, M. Vrinat, Catal. Today 86 (2003) 5.
[14] P. Rayo, J. Ancheyta, J. Ramírez, A. Gutierez-Alejandre, Catal. Today 98 (2004) 171.
[15] S.K. Maity, J. Ancheyta, L. Soberanis, F. Alonso, Appl. Catal. A 250 (2003) 231.
[16] G. Murali Dhar, B.N. Srinivas, M.S. Rana, M. Kumar, S.K. Maity, Catal. Today 86 (2003) 45.
[17] S.K. Maity, M.S. Rana, S.K. Bej, J. Ancheyta, G. Murali Dhar, T.S.R. Prasada Rao, Appl. Catal. A 205 (2001) 215.
[18] S.K. Maity, M.S. Rana, S.K. Bej, J. Ancheyta, G. Murali Dhar, T.S.R. Prasada Rao, Catal. Lett. 72 (2001) 115.
[19] M.S. Rana, S.K. Maity, J. Ancheyta, G. Murali Dhar, T.S.R. Prasada Rao, Appl. Catal. A 253 (2003) 165.
[20] M.S. Rana, J. Ancheyta, P. Rayo, S.K. Maity, Catal. Today 98 (2004) 151.
[21] B. Caloch, M.S. Rana, J. Ancheyta, Catal. Today 98 (2004) 91.
[22] H. Shimada, Catal. Today 86 (2003) 17.
[23] P.C.H. Mitchel, C.S. Scott, Catal. Today 7 (1990) 467.
[24] S. Inoue, A. Muto, H. Kudou, T. Ono, Appl. Catal. A 269 (2004) 7.
[25] M.S. Rana, J. Ancheyta, P. Rayo, Catal. Today 109 (2005) 24.
[26] M.S. Rana, J. Ancheyta, S.K. Maity, P. Rayo, Catal. Today 104 (2005) 86.
[27] M.S. Rana, M.L. Huidobro, J. Ancheyta, M.T. Gómez, Catal. Today 107–108 (2005) 346.
[28] M. Marafi, A. Stanislaus, Appl. Catal. A 159 (1997) 259.
[29] T.H. Fleisch, B.L. Meyers, J.B. Hall, G.L. Ott, J. Catal. 86 (1984) 147.
[30] B.J. Johnson, F.E. Massoth, J. Bartholdy, AIChE J. 32 (1986) 1980.
[31] S. Fukase, S. Akashah, Hydrocarbon Asia (2004) 24.
[32] B.M. Moyse, B.H. Cooper, A. Albjerg, in: Proceedings of the Am-84-59 NPRA Annual Meeting, National Petroleum Refiners Association, Texas, (1984.
[33] H. Toulhot, R. Szymanski, J.C. Plumail, Catal. Today 7 (1990) 531.
[34] C. Takeuchi, S. Asaoka, S.I. Nakata, Y. Shiroto, Preprints, ACS Div. of Petr. Chem. Symp. 30 (1985) 96.
[35] J. Bartholdy, B.H. Cooper, in: M. Absi-Halabi, et al. (Eds.), Catalyst in Petroleum Refining and Petrochemical Industries, Elsevier, Amsterdam, 1995, p. 117.
[36] C.T. Adam, A.A. del Paggio, H. Schaper, W.H.J. Store, W.K. Shiflett, Hydroc. Proc. 9 (1989) 57.
[37] J. Ancheyta, M.S. Rana, E. Furimsky, Catal. Today 109 (2005) 3.
[38] Manual Quantochrome, Nova 2000 equipment.
[39] M. Breysse, E. Furimsky, S. Kasztelan, M. Lacroix, G. Perot, Catal. Rev. Sci. Eng. 44 (4) (2002) 651.